Proceedings of ESDA2002:
6th Biennial Conference on Engineering Systems Design and Analysis
Istanbul, Turkey, July 8-11, 2002

ESDA2002/DES-024

ON THE DYNAMIC RESPONSE OF CLOSED-LOOP ROBOTIC MANIPULATORS

Haluk Erol

Faculty of Mechanical Engineering,
Technical University of Istanbul,
80191 Gümüşsuyu, Istanbul, Turkey.
Email: erolha@itu.edu.tr

Vahit Mermertaş

Faculty of Mechanical Engineering,
Technical University of Istanbul,
80191 Gümüşsuyu, Istanbul, Turkey.
Email: mermertas@itu.edu.tr

ABSTRACT

In this paper, robotic manipulator links are modeled with finite elements where each element has a uniform cross-section. Shear deformations and rotary inertia effects are taken into account in this study. Structural damping has also been included in the formulation. The dynamic response of the system has been analyzed by solving the eigenvalue problem and the modal analysis has been used to describe the behavior of the system. Considering rigid-body, elastic, normal, Coriolis and tangential accelerations result in a nonlinear structural response. Predictor-corrector procedure in connection with the Newmark method is employed for the solution of the resulting matrix differential equation. Robotic manipulator has been considered as a parallelogram linkage. Elastic displacements of end-effector are determined for different length of the links. Results of the numerical simulations were compared to tip displacement of the planar two-link manipulator. The effect of extension of the output link on the deflection has been investigated for a closed-loop parallelogram manipulator. The tip displacements in the vertical and horizontal directions decrease when the center of mass of the output link is moved away from the end-effector in both trajectories. The tip deflections were compared to the planar two-link manipulator with the parallelogram mechanism. The tip deflection produced by closed-chain manipulator is smaller and less fluctuates than those obtained for open-loop manipulator. This characteristic is more pronounced especially for horizontal trajectory.

INTRODUCTION

R.C. Winfrey [1] is one of the earliest researchers to study elastic links. A plane four-bar mechanism was used for developing the equation of motion. In his study, it was shown how the methods for determining the motion of a rigid link mechanism and methods for analyzing vibration structures might be combined, using linear theory. Iman, Sandor and Kramer [2] investigated deflections and stress analysis in four-bar planar mechanism with elastic links. The purpose of their paper was to develop a method of Kineto-elastodynamic analysis, which was applied to all planar mechanisms, and to present a method of dynamic stress analysis of mechanisms possessing elastic links. Sadler and Sandor [3] extended the lumped parameter approach to the investigation of the lateral bending vibrations of machine elements, which can be idealized as simply supported beams in planar motion. Also, stress analysis was performed with the objective of redesigning a beam of given length. Sadler [4] compared the analytical results based on non-linear differential equations derived by way of Euler-Bernoulli beam theory with experimental results. Bahgat and Willmert [5] carried out the vibration analysis of planar manipulators with links of any complex shape. They used finite element technique to evaluate the vibrations of a planar mechanism composed of links with turning and sliding pairs. The steady state solution of the resulting differential equations was obtained using a harmonic series technique. Dubowsky and Gardner [6] showed that it is possible to formulate and solve the general problem of the interaction between the effects of joint clearances and link elasticity in general planar mechanisms. Midha, Erdman and Frohrib [7] modeled the linkage with uniform cross-sectional area to define the mass and stiffness properties of a four-bar linkage. Standard structural analysis technique has been pieced together to formulate a systematic procedure for the analysis of elastic linkage. Shabana and Wehage [8] presented a method based on solving the eigenvalue problem of the substructure. From Fourier analysis of the forcing functions, an initial estimate of the number of modes to be retained was made, and during the simulation additional eigenvectors were recalled or deleted as required. Low and

Vidyasagar [9] presented a procedure for deriving dynamic equations for manipulators containing both rigid and flexible links. A two-link manipulator with one rigid link and one flexible link was analyzed to illustrate the procedure. The equations were derived using Hamilton's principle, and non-linear integro-differential equations. Benati and Morro [10] developed a Lagrangian approach for the dynamics of a chain with flexible links. Each link is modeled as a system with a finite number of degrees of freedom, one of them describing the rotation, the other ones the flexibility. Cleghorn and Chao [11] modeled four-bar mechanism with finite elements, each having linearly varying cross-sectional areas. Steady-state values of flexural strains were calculated for mechanism having prescribed link geometry, and input rotational speeds. Lee [12] formulated the equations of motion in matrix form for a flexible rod in a quick return mechanism using Hamilton's principle and the assumed mode method. Sharan and Kalra [13] carried out the dynamic analysis of finite element modeled robotic manipulators using modal analysis. Using the eigenvectors of the transposed system diagonalized the non-symmetric system matrices of the manipulators having gross motion. Shigang, Yueqing and Shixan [14] reported a new flexible rotor beam element to study the dynamic behavior of manipulators with flexible links and joints. Both link and joint flexibility were incorporated together by using the finite element model for links and a torsional spring model for joints. A planar 3R manipulator with flexible links and joints was analyzed as an example. Boyer and Khalil [15] presented an exact expression of the finite rotation field directly deduced from the centerline displacement and torsion fields of a slender beam and applied that result to the calculation of the kinematical model of an open chain flexible multi-body system subjected to large displacements. Siciliano [16] presented an inverse kinematics scheme for a planar two-link flexible manipulator under gravity whose tip is considered by a stiff surface. The computed joint and deflection displacements were used as the set point for PD control.

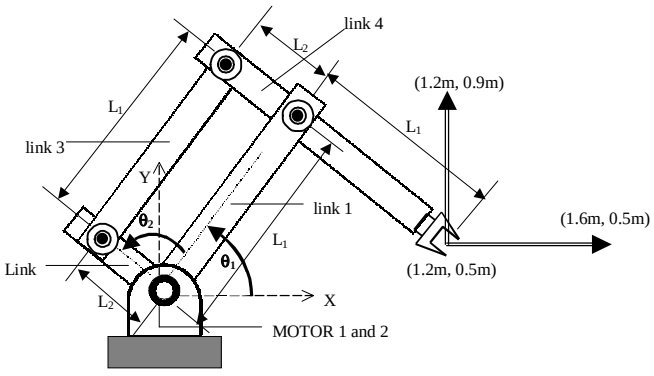

Figure 1. The planar manipulator with parallelogram mechanism and the trajectory.

In the present study, the robotic manipulator was considered as a parallelogram linkage shown in Figure 1.

The links were taken as beams with shear deformation. The elastic displacements of end-effector in x and y directions were determined for different length of the links using the finite element method. Results of the numerical simulations are compared to tip displacement of the planar two-link manipulator shown in Figure 2.

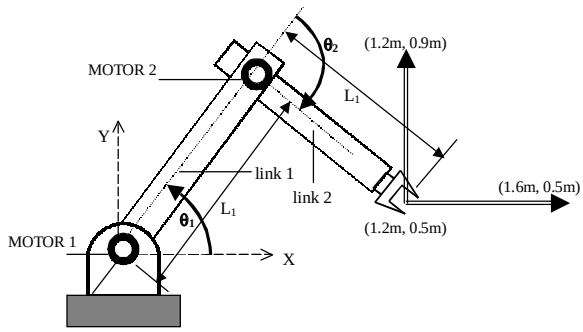

Figure 2. The planar two-link manipulator and the trajectory.

BEAM ELEMENT IN PLANE MOTION

The links of the manipulator taken as general beam elements is shown in Figure 3. There are two coordinate systems. These are the fixed (OXY) and the rotating (Oxy) coordinate systems. The elastic translations and rotations relative to the rotating (Oxy) frame as the x-axis are parallel to the beam element axis as shown in Figure 3.

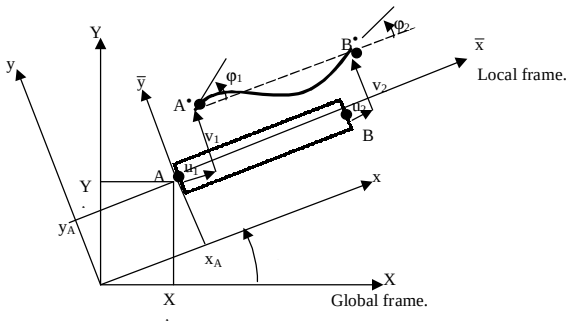

Figure 3. Deflection variables of the flexible element and the coordinate systems.

The elastic deformations of the beam element are described by six nodal displacements. These are the transverse and longitudinal deflections, rotations at each end of the element. The following relationships may be written in fixed coordinate system.

$$
\begin{aligned}
X_{A^*} &= X_A + u_1\cos\varphi - v_1\sin\varphi \\
Y_{A^*} &= Y_A + u_1\sin\varphi + v_1\cos\varphi \\
\varphi_{A^*} &= \varphi + \varphi_1
\end{aligned} \tag{1}
$$

where, X_A, Y_A and ϕ describe the rigid-body motion of the element. Differentiating equation (1) twice with respect to time, absolute accelerations of A^* may be obtained in fixed coordinate system.

$$
\begin{aligned}
\ddot{X}_{A^*} &= \ddot{X}_A + \ddot{u}_1\cos\varphi - 2\dot{u}_1\dot{\varphi}\sin\varphi - u_1\dot{\varphi}^2\cos\varphi - u_1\ddot{\varphi}\sin\varphi \\
&\quad - \ddot{v}_1\sin\varphi - 2\dot{v}_1\dot{\varphi}\cos\varphi + v_1\dot{\varphi}^2\sin\varphi - v_1\ddot{\varphi}\cos\varphi \\
\ddot{Y}_{A^*} &= \ddot{Y}_A + \ddot{u}_1\sin\varphi + 2\dot{u}_1\dot{\varphi}\cos\varphi - u_1\dot{\varphi}^2\sin\varphi + u_1\ddot{\varphi}\cos\varphi \\
&\quad + \ddot{v}_1\cos\varphi - 2\dot{v}_1\dot{\varphi}\sin\varphi - v_1\dot{\varphi}^2\cos\varphi - v_1\ddot{\varphi}\sin\varphi \\
\ddot{\varphi}_{A^*} &= \ddot{\varphi} + \ddot{\varphi}_1
\end{aligned} \tag{2}
$$

The absolute and rigid body accelerations of the element are expressed in the rotating frames with the help of following transformations.

$$
\begin{aligned}
\ddot{x}_{A^*} &= \ddot{X}_{A^*}\cos\varphi + \ddot{Y}_{A^*}\sin\varphi \\
\ddot{y}_{A^*} &= -\ddot{X}_{A^*}\sin\varphi + \ddot{Y}_{A^*}\cos\varphi \\
\ddot{x}_A &= \ddot{X}_A\cos\varphi + \ddot{Y}_A\sin\varphi \\
\ddot{y}_A &= -\ddot{X}_A\sin\varphi + \ddot{Y}_A\cos\varphi
\end{aligned} \tag{3}
$$

By combining equation (2) and equation (3) and performing the similar procedure for node B, one obtains:

$$
\begin{Bmatrix} \ddot{x}_{A^*} \\ \ddot{y}_{A^*} \\ \ddot{\varphi}_{A^*} \\ \ddot{x}_{B^*} \\ \ddot{y}_{B^*} \\ \ddot{\varphi}_{B^*} \end{Bmatrix} = \begin{Bmatrix} \ddot{x}_A \\ \ddot{y}_A \\ \ddot{\varphi}_A \\ \ddot{x}_B \\ \ddot{y}_B \\ \ddot{\varphi}_B \end{Bmatrix} + \begin{Bmatrix} \ddot{u}_1 \\ \ddot{v}_1 \\ \ddot{\varphi}_1 \\ \ddot{u}_2 \\ \ddot{v}_2 \\ \ddot{\varphi}_2 \end{Bmatrix} + \begin{bmatrix} 0 & -2\dot{\varphi} & 0 & 0 & 0 & 0 \\ 2\dot{\varphi} & 0 & 0 & 0 & 0 & 0 \\ 0 & 0 & 0 & 0 & 0 & 0 \\ 0 & 0 & 0 & 0 & -2\dot{\varphi} & 0 \\ 0 & 0 & 0 & 2\dot{\varphi} & 0 & 0 \\ 0 & 0 & 0 & 0 & 0 & 0 \end{bmatrix} \begin{Bmatrix} \dot{u}_1 \\ \dot{v}_1 \\ \dot{\varphi}_1 \\ \dot{u}_2 \\ \dot{v}_2 \\ \dot{\varphi}_2 \end{Bmatrix}
$$

$$
+ \begin{bmatrix} -\dot{\varphi}^2 & -\ddot{\varphi} & 0 & 0 & 0 & 0 \\ \ddot{\varphi} & -\dot{\varphi}^2 & 0 & 0 & 0 & 0 \\ 0 & 0 & 0 & 0 & 0 & 0 \\ 0 & 0 & 0 & -\dot{\varphi}^2 & -\ddot{\varphi} & 0 \\ 0 & 0 & 0 & \ddot{\varphi} & -\dot{\varphi}^2 & 0 \\ 0 & 0 & 0 & 0 & 0 & 0 \end{bmatrix} \begin{Bmatrix} u_1 \\ v_1 \\ \varphi_1 \\ u_2 \\ v_2 \\ \varphi_2 \end{Bmatrix} \tag{4}
$$

where the matrix (from left to right) represent the absolute, rigid-body, elastic, normal, Coriolis and tangential accelerations. The last two vectors in equation (4) are the rigid-body and elastic motions coupling terms.

MASS AND STIFFNESS MATRICES

It is assumed that the dynamic axial forces are not large enough to affect the flexural stiffness, there is no coupling between the axial and flexural stiffness. The appropriate energy expressions for the element shown in Figure 3 are from reference [20].

$$
\begin{aligned}
T &= \frac{1}{2}\int_0^L \rho A\, \dot{u}(\bar{x},t)^2\, d\bar{x} + \frac{1}{2}\int_0^L \rho A\, \dot{v}(\bar{x},t)^2\, d\bar{x} \\
&\quad + \frac{1}{2}\int_0^L \rho I_z\, \dot{\varphi}(\bar{x},t)^2\, d\bar{x},
\end{aligned} \tag{5}
$$

$$
\begin{aligned}
U &= \frac{1}{2}\int_0^L E A\, u'(\bar{x},t)^2\, d\bar{x} + \frac{1}{2}\int_0^L E I_z\, \varphi'(\bar{x},t)^2\, d\bar{x} \\
&\quad + \frac{1}{2}\int_0^L \kappa A G\left(v'(\bar{x},t) - \varphi(\bar{x},t)\right)^2\, d\bar{x}
\end{aligned} \tag{6}
$$

The displacement functions can be represented by a polynomial having constants, namely

$$
v(\bar{x}) = \left(a_1 + a_2\,\bar{x} + a_3\bar{x}^2 + a_4\bar{x}^3\right) \tag{7}
$$

$$
\varphi(\bar{x}) = \left(b_1 + b_2\,\bar{x} + b_3\bar{x}^2\right) \tag{8}
$$

$$
u(\bar{x}) = \left(c_1 + c_2\,\bar{x}\right) \tag{9}
$$

These seven constants of the integration are not independent since the solutions (7) and (8) must also satisfy moment equilibrium equation. This gives the following relationships:

$$
b_1 = \frac{2}{L}a_2 + \frac{12\beta}{L}a_4, \quad b_2 = \frac{4}{L}a_3, \quad b_3 = \frac{6}{L}a_4 \tag{10}
$$

where

$$
\beta = \frac{4 E I_z}{\kappa A G L^2} \tag{11}
$$

Substituting the displacement functions into the energy expressions gives the element matrices.

The elemental mass and stiffness matrices can then be transformed into a global coordinate frame.

$$
\begin{aligned}
[m] &= [R]^T\,[\bar{m}]\,[R], \\
[k] &= [R]^T\,[\bar{k}]\,[R]
\end{aligned} \tag{12}
$$

where [R] represents the elemental transformation matrix from local to global coordinates frame, $[\overline{m}]$ and $[\overline{k}]$ are the element mass and stiffness matrices. Elemental matrices and transformation matrix are given in the Appendix.

DAMPING AND MODAL ANALYSIS

By equating the energy in the total manipulator to the sum of the energy in each link and after applying corresponding boundary conditions the differential equations of motion can be written in the matrix form,

$$[M]\{\ddot{q}(t)\}+[C]\{\dot{q}(t)\}+[K]\{q(t)\}=\{Q(t)\} \qquad (13)$$

where [M] and [K] are the system mass, stiffness matrices. $\{\ddot{q}_R(t)\}$ is the vector of the rigid-body accelerations. The damping matrix cannot be constructed from element damping matrix, such as the mass and stiffness matrices of the element assemblage. The damping matrix associated with any given set of modal damping ratios ξ_n can be obtained by pre-and post-multiplying the diagonal matrix of the generalized damping coefficients by the inverse of the mode-shape matrix or its transpose [17].

$$[C]=[[U]^T]^{-1}\begin{bmatrix} 2\xi_1\omega_1 & 0 & 0 & \cdots \\ 0 & 2\xi_2\omega_2 & 0 & \cdots \\ 0 & 0 & 2\xi_3\omega_3 & \cdots \\ \cdots & \cdots & \cdots & \cdots \end{bmatrix}[U]^{-1}, \qquad (14)$$

$$[U]^T[M][U]=[I],$$

$$[U]^T[K][U]=[\omega_r^2], \qquad (15)$$

where [U] is the normalized modal matrix and $[\omega_r^2]$ is the diagonal matrix of the natural frequencies squared of the undamped system.

The orthogonal properties of the modal coordinates may be used to simplify the equations of motion the multi-degree of freedom system. Equation (13) may be written by considering the linear transformation

$$\{q(t)\}=[U]\{\eta(t)\}, \qquad (16)$$

relating the vectors $\{q(t)\}$ and $\{\eta(t)\}$, where these vectors represent two different sets of generalized coordinates. Introducing transformation equation (16) into equation (13), pre-multiplying the result by $[U]^T$ and considering equation (14) and equation (15),

$$\{\ddot{\eta}(t)\}+[2\xi\omega]\{\dot{\eta}(t)\}+[\omega^2]\{\eta(t)\}=\{N(t)\}. \qquad (17)$$

The amplitudes of the higher modes of the system are usually negligible compared to the first few modes. The computational efficiency would be increased if the lower modes were calculated rather than all modes. In such a case, modal matrix can be written as,

$$[U]=[\{U\}_1,\{U\}_2,.....\{U\}_m], \qquad (18)$$

where m is the number of modes to be used in the solution. In this finite element solution 10 modes are considered. Sharan and Kalra [13] used only 4 modes to describe the system behavior for planar two-link manipulator. Equation (19) represents a set of n independent equations of the form,

$$\ddot{\eta}_r(t)+2\xi_r\omega_r\dot{\eta}_r(t)+\omega_r^2\eta_r(t)=N_r(t), \qquad (19)$$

where $\eta_r(t)$ are recognized as the system modal coordinates and $N_r(t)$ are associated modal generalized forces. Equation (19) has the same structure as the differential equation of motion of a single-degree-of freedom system.

THE PREDICTOR-CORRECTOR SCHEME

In the Newmark integration scheme the equilibrium equation (19) is considered at time t+Δt,

$$\ddot{\eta}_r(t+\Delta t)+2\xi_r\omega_r\dot{\eta}_r(t+\Delta t)+\omega_r^2\eta_r(t+\Delta t)=N_r(t+\Delta t)$$
$$r = 1,2, \ldots, m \qquad (20)$$

where $\eta_r(t+\Delta t)$ is the r^{th} generalized modal displacement at time t+Δt. The finite difference representation of displacement and velocity based on the Newmark method, can be written as

$$\dot{\eta}_r(t+\Delta t)=\dot{\eta}_r(t)+[(1-\delta)\ddot{\eta}_r(t)+\delta\ddot{\eta}_r(t+\Delta t)]\Delta t \qquad (21)$$

$$\eta_r(t+\Delta t)=\eta_r(t)+\dot{\eta}_r(t)\Delta t+[(1/2-\alpha)\ddot{\eta}_r(t)+\alpha\ddot{\eta}_r(t+\Delta t)]\Delta t^2 \qquad (22)$$

where δ and α are parameters to be chosen to obtain optimum stability and accuracy. Newmark in reference [19], proposed as an unconditionally stable scheme the constant-average-acceleration method, in which case $\delta \geq 0.5$ and $\alpha \geq 0.25(0.5+\delta)^2$.

To initiate the predictor-corrector process within the current time step, a value for $\ddot{\eta}_r(t+\Delta t)$ in equation (20) needs to be assumed. This value may be designed as ${}^o\ddot{\eta}_r(t+\Delta t)$ and can be taken as zero, where superscript "o" is the initial value of the

predictor-corrector iteration index i. On this basis, from equation (21) and equation (22), ${}^{o}\dot{\eta}_r(t+\Delta t)$ and ${}^{o}\eta_r(t+\Delta t)$ can be computed as

$$ {}^{o}\dot{\eta}_r(t+\Delta t) = \dot{\eta}_r(t) + (1-\delta)\ddot{\eta}_r(t)\Delta t \qquad (23) $$

$$ {}^{o}\eta_r(t+\Delta t) = \eta_r(t) + \dot{\eta}_r(t)\Delta t + (1/2-\alpha)\ddot{\eta}_r(t)\Delta t^2, \qquad (24) $$

with values of ${}^{o}\ddot{\eta}_r(t+\Delta t)$, ${}^{o}\dot{\eta}_r(t+\Delta t)$ and ${}^{o}\eta_r(t+\Delta t)$, it is now necessary to determine the corresponding force in equation (20). At this point, from an implementation perspective, it becomes convenient to update the iteration index i, and start the predictor-corrector loop. The predicted values of ${}^{i-1}\ddot{\eta}_r(t+\Delta t)$, ${}^{i-1}\dot{\eta}_r(t+\Delta t)$, ${}^{i-1}\eta_r(t+\Delta t)$ and ${}^{i-1}N_r(t+\Delta t)$ do not identically satisfy the governing equation. Equation (20) is evaluated to determine whether there is any residual force in the system. The residual force is

$$ {}^{i-1}\Delta N_r(t+\Delta t) = {}^{i-1}N_r(t+\Delta t) - \left[{}^{i-1}\ddot{\eta}_r(t+\Delta t) + 2\xi_r\omega_r\, {}^{i-1}\dot{\eta}_r(t+\Delta t) + \omega_r^2\, {}^{i-1}\eta_r(t+\Delta t) \right]. \qquad (25) $$

If ${}^{i-1}\Delta N_r(t+\Delta t)$ is within a specified tolerance, the process is halted. Otherwise, the correction procedure is continued. The predicted values of ${}^{i-1}\ddot{\eta}_r(t+\Delta t)$, ${}^{i-1}\dot{\eta}_r(t+\Delta t)$ and ${}^{i-1}\eta_r(t+\Delta t)$ can then be corrected in accordance with equation (26).

Substituting for $\dot{\eta}_r(t+\Delta t)$ and $\eta_r(t+\Delta t)$ into equation (20), we can solve for $\ddot{\eta}_r(t+\Delta t)$ and then use equation (21) and equation (22) to calculate $\dot{\eta}_r(t+\Delta t)$ and $\eta_r(t+\Delta t)$. Thus the relation can be established as,

$$ \begin{Bmatrix} {}^{i}\ddot{\eta}_r(t+\Delta t) \\ {}^{i}\dot{\eta}_r(t+\Delta t) \\ {}^{i}\eta_r(t+\Delta t) \end{Bmatrix} = [P] \begin{Bmatrix} \ddot{\eta}_r(t) \\ \dot{\eta}_r(t) \\ \eta_r(t) \end{Bmatrix} + [Y]\, {}^{i-1}N_r(t+\Delta t), \qquad (26) $$

where

$$ [P] = \begin{bmatrix} -(1/2-\alpha A)\lambda - 2(1-\delta)\mu & (-\lambda - 2\mu)/\Delta\Delta & -\lambda/\Delta t^2 \\ \Delta t[1-\delta-(1/2-\alpha)\delta\lambda - 2(1-\delta)\delta\mu] & 1-\lambda\delta - 2\delta\mu & -\lambda\delta/\Delta t \\ \Delta t^2[1/2-\alpha-(1/2-\alpha)\alpha\lambda - 2(1-\delta)\alpha\mu] & \Delta t(1-\alpha\lambda - 2\alpha\mu) & (1-\alpha\lambda) \end{bmatrix} \qquad (27) $$

$$ \lambda = \left(\frac{1}{\omega_r^2\,\Delta t^2} + \frac{2\xi\delta}{\omega_r\,\Delta t} + \alpha \right)^{-1}, \qquad \mu = \frac{\xi\lambda}{\omega_r\,\Delta t}, \qquad (28) $$

and

$$ [Y] = \begin{Bmatrix} \dfrac{\lambda}{\omega_r^2\,\Delta t^2} \\ \dfrac{\lambda\delta}{\omega_r^2\,\Delta t} \\ \dfrac{\alpha\lambda}{\omega_r^2} \end{Bmatrix}. \qquad (29) $$

To initiate the predictor-corrector process needs the initial modal displacements $\eta_r(0)$ and velocities $\dot{\eta}_r(0)$, which are related to the actual initial displacements $q_r(0)$ and velocities $\dot{q}_r(0)$. Pre-multiplying equation (16) by $[U]^T[M]$ and considering the orthogonal properties of the modal vectors, the initial modal displacements and velocities can be determined as follows,

$$ \{\eta(0)\} = [U]^T[M]\{q(0)\}, $$
$$ \{\dot{\eta}(0)\} = [U]^T[M]\{\dot{q}(0)\}. \qquad (30) $$

Hence, the complete solution of equation (13) can be obtained by inserting the modal coordinates equation (26) into equation (16).

The solutions of equation (13) are dependent on the [M], [K] and [C] matrices, which are determined by input angles. Hence the trajectory can be divided into segments over which the system mass, damping and stiffness matrices are constant. The solution at the end of a segment would be the initial conditions for the next segment. In the mathematical algorithm presented in this paper, the trajectory is divided into ten segments.

NUMERICAL SIMULATIONS

Figure 2 shows a manipulator arm consisting of a closed-loop planar parallelogram mechanism. One actuator is fixed to the base link; the other is fixed to the link 1 and drives the two input links. Link 4 is the output link, where an end-effector is attached.

The motion profile was created using the following equations:

$$ \theta_i = \Theta_i \left[\frac{t}{T_0} - \frac{1}{2\pi}\sin\left(\frac{2\pi t}{T_0} \right) \right], \qquad (31) $$

where T_0 is the total time of the trajectory (1.4s) and Θ is the magnitude of rotation. The beams are uniform with cross-section of 10mm x 15 mm, mass per unit length 1.17 kg/m, moment of inertia $2.8125\text{x}10^{-9}$ m^4 and made of material that gives a modulus of elasticity $2.1\text{x}10^{11}$ N/m^2. The mass of the motor is taken as 5 kg.

To verify the theoretical model, the manipulator is divided into twenty elements. The trajectory is divided into ten segments over which the system mass, damping and stiffness matrices are constant. Ten modes are considered to describe the system behavior for parallelogram and two-link manipulator. Several examples are solved to illustrate the effects of the length of the output link and trajectory of the endpoint on the tip deflection in the vertical and horizontal direction. The results are presented in a series of Figures plotted in term of the oscillation time. All links of the manipulators shown in Figure 1 and 2 were considered to be flexible and the tip deflections are determined with the effect of gravitational forces.

Numerical examples are separated into two parts. The first part deals with the endpoint trajectory that is simulated by prescribing certain horizontal motion from point (1.2m, 0.5m) to (1.2m, 0.9m), while the second part treats the problem using prescribed vertical direction from point (1.2m, 0.5m) to (1.6m, 0.5m). The results of the first part can be seen in Figure 4-7 and the results of second part are plotted in Figure 8-11.

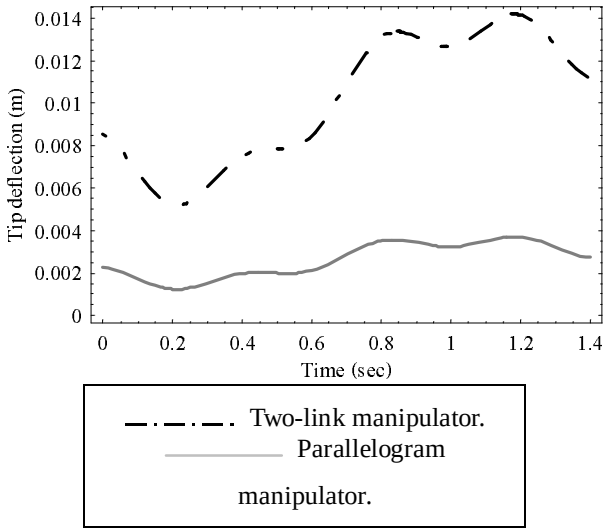

Figure 4. Tip deflections of manipulator with parallelogram mechanism and two-link manipulator for horizontal trajectory in x direction. (L_1= 0.9m, L_2= 0.3m).

In order to investigate the effects of the length of the output link, the length of L_2 is varied from 0.1m to 0.5 m, while the other lengths of the manipulator are kept constant at 0.9m. The tip deflections are presented in Figure 6,7,10,11. Comparison of these Figures shows that deflections of closed-loop manipulator with short and long extension of the output link are quite different, although other lengths are the same in all cases. The tip displacement in the vertical and horizontal direction decreases when the center of mass of the output link is moved away from the end-effector in both trajectories.

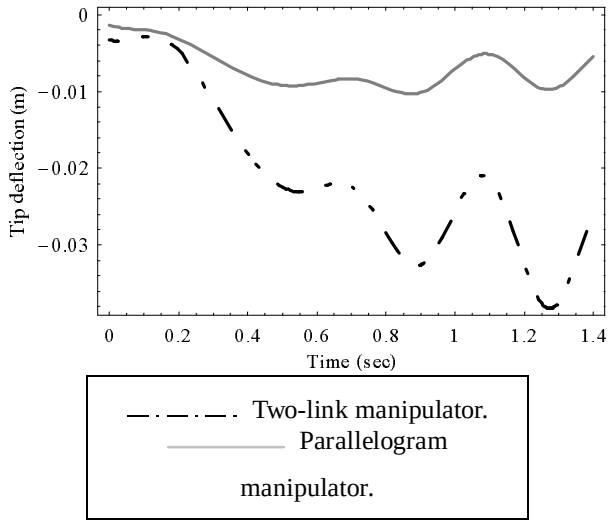

Figure 5. Tip deflections of manipulator with parallelogram mechanism and two-link manipulator for horizontal trajectory in y direction. (L_1= 0.9m, L_2= 0.3m).

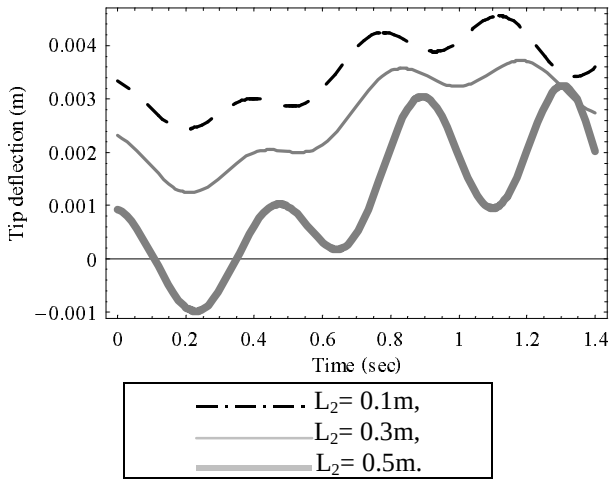

Figure 6. Tip deflections of manipulator with parallelogram mechanism for horizontal trajectory in x direction. (L_1= 0.9m).

The deflections for the closed-loop manipulator for the case of L_2 = 0.3m with the present model are compared with the results of planar two-link manipulator with the same length of the other links (L_1 = 0.9m) in Figure 4,5,8,9. It can be seen from these Figures that the tip deflection produced by closed-chain manipulator are smaller and fluctuate less than those obtained for open-loop manipulator in both trajectory. This verifies the fact that this type of planar two-link manipulators presents drawback. Their elastic flexibility is high due to the cantilever-type of their links. Flexibility introduces positioning inaccuracies and undesired dynamical side effects because only one of the motors is fixed, the remaining one, accounting for a substantial part of the inertial load is moving.

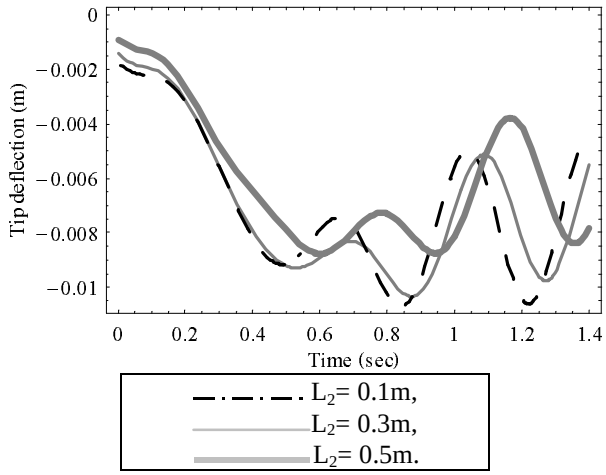

Figure 7. Tip deflections of manipulator with parallelogram mechanism for horizontal trajectory in y direction. (L1 = 0.9 m).

It can also be observed from Figure 4 and 5 that, the difference between the deflection curve of closed and open-loop manipulators increases while the time reaches to the end of the trajectory time in both directions for horizontal trajectory. However, the difference is less remarkable for vertical trajectory shown in Figure 8 and 9.

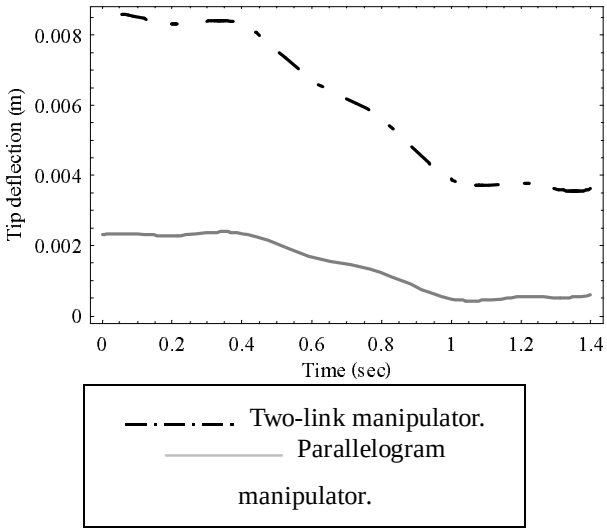

Figure 8. Tip deflections of manipulator with parallelogram mechanism and two-link manipulator for vertical trajectory in x direction. (L_1= 0.9m, L_2= 0.3m).

The residual vibrations behave after the time is reached to the end of the trajectory time. The motion is the result of initial conditions, which is equal to the final conditions at the end of this time. At that point damped free vibrations will occur since there is loss energy throughout the motion of the system.

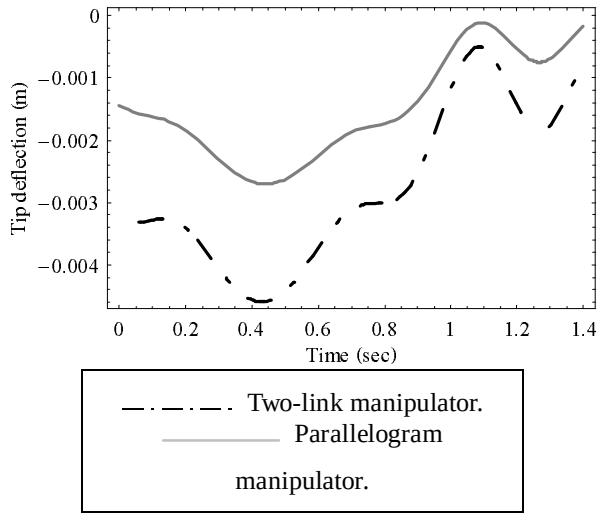

Figure 9. Tip deflections of manipulator with parallelogram mechanism and two-link manipulator for vertical trajectory in y direction. (L_1= 0.9m, L_2= 0.3m).

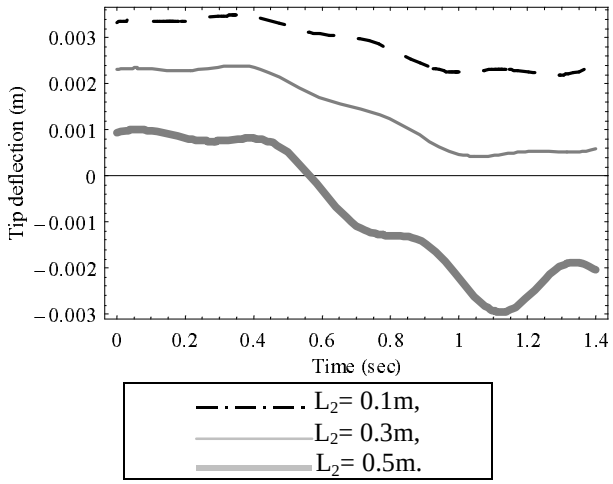

Figure 10. Tip deflections of manipulator with parallelogram mechanism for vertical trajectory in x direction. (L_1= 0.9m).

CONCLUSIONS

The dynamic behavior of planar a manipulator with parallelogram mechanism has been analyzed theoretically by means of the finite element method with the effect of damping taken into account. Each element has a uniform cross-section. Shear deformation and rotary inertia effects have also been included in the formulation. The consideration of rigid-body, elastic, normal, Coriolis and tangential accelerations results in a nonlinear structural response. Predictor-corrector procedure in connection with the Newmark method is employed for the solution of the resulting matrix differential equation. The trajectory is divided into ten segments over which the mass,

stiffness and damping matrices are constant. The modal analysis has been used to describe the system behavior. Ten modes are considered for calculation of tip deflection in horizontal and vertical trajectory.

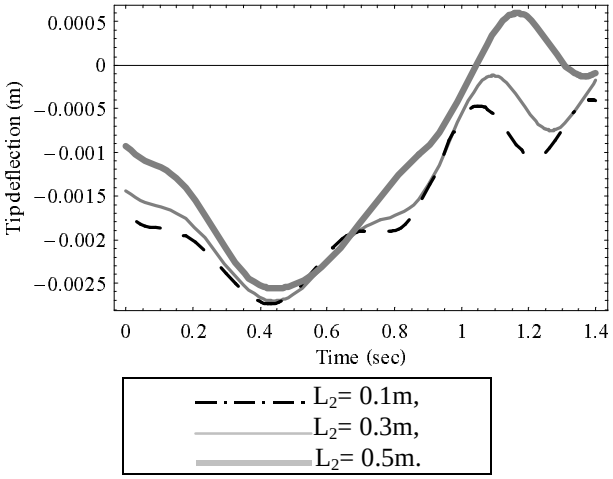

Figure 11. Tip deflections of manipulator with parallelogram mechanism for vertical trajectory in y direction. (L_1= 0.9m).

The effect of extension of the output link on the deflection has been investigated for a closed-loop parallelogram manipulator. The tip displacement in the vertical and horizontal direction decreases when the center of mass of the output link is moved away from the end-effector in both trajectories.

The tip deflections are compared to the planar two-link manipulator with the parallelogram mechanism. The tip deflection produced by closed-chain manipulator is smaller and less fluctuates than those obtained for open-loop manipulator. This characteristic is more pronounced especially for horizontal trajectory.

ACKNOWLEDGMENTS

The Young Researchers Support Program of Istanbul Technical University sponsored this study. Authors are grateful for this financial support.

REFERENCES

[1] Winfrey, R.C., 1971, "Elastic link mechanism design", Journal of Engineering for Industry, 268-272.

[2] Iman, I., Sandor, G., and Kramer, S.N., 1973, "Deflection and stress analysis in high-speed planar mechanisms with elastic links", Journal of Engineering for Industry, 541-547.

[3] Sadler, J.P., and Sandor, G.N., 1973, "A lumped parameter approach to vibration and stress analysis of elastic linkages", Journal of Engineering for Industry, 541-547.

[4] Sadler, J.P., 1975, "On the analytical lumped-mass model of an elastic four-bar mechanism", Journal of Engineering for Industry, 561-565.

[5] Bahgat, B.M., and Willmert, K.D., 1976, "Finite element vibrational analysis of planar mechanism", Mechanism and Machine Theory, **11**, 14-71.

[6] Dubowsky, S., and Gardner, T.N., 1975, "Dynamic interaction of link elasticity and clearance connections in planar mechanical system", Journal of Engineering for Industry, 652-661.

[7] Midha, A., Erdman, A.G., and Frohrib, D.A., 1978, "Finite element approach to modeling of high-speed elastic linkages", Mechanism and Machine Theory, **13**, 603-618.

[8] Shabana, A., and Wehage, R.A., 1983, "Variable degree-of-freedom component mode analysis of inertia variant flexible mechanical system", Journal of Mechanism, Transmissions, and Automation in Design, **105**, 371-377.

[9] Low, K.H., and Vidyasagar, M., 1988, "A lagrangian formulation of the dynamic modal for flexible manipulator systems", Journal of Dynamic Systems, Measurement, and Control, **110**, 175-181.

[10] Benati, M., and Morro, A., 1988, "Dynamic of chain of flexible links", Journal of Dynamic Systems, Measurement, and Control, **110**, 410-415.

[11] Cleghorn, W.L., and Chao, K.C., 1988, "Kineto-elastodynamic modeling of mechanisms employing linearly tapered beam finite elements", Mechanism and Machine Theory, **23**, 333-342.

[12] Lee, H.P., 1994, "Dynamic of a flexible rod in a quick return mechanism", Journal of Mechanical Design, **116**, 70-74.

[13] Sharan, A.M., and Kalra, P., 1994, "Dynamic response of robotic manipulators using modal analysis", Mechanism and Machine Theory, **29**, 1233-1249.

[14] Shigang, Y., Yueqing, Y., and Shixan, B., 1997, "Flexible rotor beam for the manipulators with joint and link flexibility", Mechanism and Machine Theory, **32**, 209-219.

[15] Boyer, F., and Khalil, W., 1999, "Kinematic model of a multi-beam structure undergoing large elastic displacements and rotations. Part two: kinematic model of an open chain", Mechanism and Machine Theory, **34**, 223-242.

[16] Siciliano, B., 1999, "Closed-loop inverse kinematics algorithm for constrained flexible manipulators under gravity", Journal of Robotic Systems, **16**, 353-362.

[17] Clough, R.W., and Penzien, J., 1975, Dynamic of Structures, McGraw-Hill, New-York.

[18] Meirovitch, L., 1986, Elements of Vibration Analysis. McGraw-Hill, Singapore.

[19] Bathe, K.J. and Wilson, E.L., 1976, Numerical Methods in Finite Element Analysis Prentice-Hall, Englewood Cliffs, NJ.

[20] Petyt, M., Introduction to Finite Element Vibration Analysis, Cambridge University Press, Avon.

APPENDIX

The mass and stiffness matrices for a uniform element are

$$[\overline{m}] = \frac{\rho A L}{420(1+3\beta)^2}\begin{bmatrix} 0 & & & & & \\ 0 & m_1 & & \text{sym.} & & \\ 0 & m_2 & m_5 & & & \\ 0 & 0 & 0 & 0 & & \\ 0 & m_3 & -m_4 & 0 & m_1 & \\ 0 & m_4 & m_6 & 0 & -m_2 & m_5 \end{bmatrix}$$

$$+\frac{\rho I_z}{15L(1+3\beta)^2}\begin{bmatrix} 0 & & & & & \\ 0 & m_7 & & \text{sym.} & & \\ 0 & m_8 & m_9 & & & \\ 0 & 0 & 0 & 0 & & \\ 0 & -m_7 & -m_8 & 0 & m_7 & \\ 0 & m_8 & m_{10} & 0 & -m_8 & m_9 \end{bmatrix}$$

$$+\rho A L\begin{bmatrix} 1/3 & & & & & \\ 0 & 0 & & \text{sym.} & & \\ 0 & 0 & 0 & & & \\ 1/6 & 0 & 0 & 1/3 & & \\ 0 & 0 & 0 & 0 & 0 & 0 \end{bmatrix}$$

where

$$m_1 = 156 + 882\,\beta + 1260\,\beta^2$$
$$m_2 = (\,44 + 231\,\beta + 315\,\beta^2\,)\,(L/2)$$
$$m_3 = 54 + 378\,\beta + 630\,\beta^2$$
$$m_4 = (\,-26 - 189\,\beta - 315\,\beta^2\,)\,(L/2)$$
$$m_5 = (\,16 + 84\,\beta + 126\,\beta^2\,)\,(L/2)^2$$
$$m_6 = (\,-12 - 84\,\beta - 126\,\beta^2\,)\,(L/2)^2$$
$$m_7 = 18$$
$$m_8 = (3 - 45\,\beta\,)\,(L/2)$$
$$m_9 = (\,8 + 30\,\beta + 180\,\beta^2\,)\,(L/2)^2$$
$$m_{10} = (\,-2 - 30\,\beta + 90\,\beta^2\,)\,(L/2)^2$$